AIAA JOURNAL
Vol. 33, No. 1, January 1995

Application of Wall Functions to Generalized Nonorthogonal Curvilinear Coordinate Systems

Douglas L. Sondak*
NASA Ames Research Center, Moffett Field, California 94035
and
Richard H. Pletcher†
Iowa State University, Ames, Iowa 50011

A method has been developed for the application of wall functions to generalized curvilinear coordinate systems with nonorthogonal grids. Two test cases have been computed using this method with the k-ϵ turbulence model: flow over a flat plate at 0-deg angle of attack using a nonorthogonal grid at the wall and flow over a prolate hemispheroid with a hemispherical nose cap at 0-deg angle of attack. All results are compared with experimental data. In addition, the hemispheroid results are compared with computations using the Baldwin-Lomax algebraic turbulence model and the Chien low-Reynolds-number k-ϵ turbulence model.

Nomenclature

B	= constant for law of the wall, 5.0
b	= proportionality constant between metrics
C_f	= friction coefficient
C_1	= constant for k-ϵ model, 1.44
C_2	= constant for k-ϵ model, 1.92
c_l	= constant for Norris and Reynolds near-wall length scale equation, 2.5
c_p	= specific heat at constant pressure
c_μ	= constant for k-ϵ model, 0.09
$\boldsymbol{G}$	= metric matrix
$g_{\alpha\beta}$	= metric tensor
H_t	= source term vector for k-ϵ equations
J	= Jacobian of coordinate transformation
k	= turbulent kinetic energy
L	= reference length
l_ϵ	= near-wall length scale of Norris and Reynolds
n	= normal distance from wall
$\boldsymbol{P}$	= physical shear stress matrix
$\mathcal{P}$	= rate of production of turbulent kinetic energy
p	= static pressure
Q	= dependent variable vector
Re	= Reynolds number, $a_\infty L/\nu_\infty$
Re_t	= turbulent Reynolds number, $\sqrt{k}n/\nu$
Re_x	= Reynolds number based on freestream velocity and distance from virtual origin
$\boldsymbol{r}$	= position vector
S	= diagonal matrix containing functions of metrics
$\boldsymbol{T}$	= shear stress matrix
t	= time
U, V, W	= contravariant velocity components
u	= velocity parallel to wall (two-dimensional examples)
u, v, w	= velocity components in Cartesian coordinate directions
u^+	= velocity normalized by friction velocity
u_*	= friction velocity
$u(\alpha)$	= physical velocity component in α direction
x, y, z	= Cartesian coordinate directions
y	= coordinate direction normal to wall (two-dimensional examples)
y^+	= distance from wall in wall coordinates
y_c^+	= point where viscous sublayer intersects log region, neglecting buffer region
γ	= coordinate direction normal to wall
δ	= boundary-layer thickness
δ_{ij}	= Kronecker delta
ϵ	= dissipation rate of turbulent kinetic energy
κ	= von Kármán constant, 0.41
μ	= molecular viscosity
μ_t	= turbulent viscosity
ξ, η, ζ, τ	= transformed coordinates
ρ	= density
σ_k	= constant for k-ϵ model, 1.0
σ_ϵ	= constant for k-ϵ model, 1.3
τ	= shear stress; transformed time in Eq. (1)
$\tau(\alpha\beta)$	= physical shear stress component in α, β directions
$\tilde{(\ )}$	= tensor in transformed coordinates
$\bar{(\ )}$	= modified by wall functions
$\hat{(\ )}$	= vector in transformed coordinates, conservation law form

Subscripts and Superscripts

t	= turbulent
v	= viscous
w	= wall
∞	= freestream condition

Introduction

THE standard high-Reynolds-number k-ϵ model requires modification for flow near walls to account for damping of velocity fluctuations normal to the wall and for viscous effects. Three common approaches are the addition of low-Reynolds-number terms, patching in a simpler model near the wall, and using wall functions.

In low-Reynolds-number models, terms are added to the standard model, some of which typically contain exponential damping functions.[1,2] These models require fine grid resolution near the walls, resulting in a relatively large total number of grid points. The equations are difficult to solve numerically due to their stiffness,[3] and results from these models are often disappointing when compared with experimental data.[4–6]

A second approach is to patch in a simpler model at the wall, such as an algebraic model or a one-equation model. This method has been shown to yield good results for some flowfields,[7–9] but more testing is required before it may be fully assessed. A disadvantage of the patched models is that they also require fine grid spacing at the wall.

Received Oct. 1, 1993; revision received June 1, 1994; accepted for publication June 1, 1994.

*Research Scientist, MCAT Institute; currently Research Engineer, Fluid Mechanics, United Technologies Research Center, East Hartford, CT 06108. Member AIAA.

†Professor, Department of Mechanical Engineering. Member AIAA.

A third approach is to use wall functions. The idea behind wall functions is that knowledge of the basic structure of turbulent boundary layers may be applied to flow near walls. The entire turbulent boundary layer need not be resolved, and a large grid spacing may be used at the wall. Since the rate at which the grid may stretch away from the wall is limited by most numerical solution schemes, wall functions result in a large saving in the total number of grid points required. Viegas and Rubesin[3] found that approximately half as many grid points were required when using wall functions as compared with low-Reynolds-number models. The reduced memory and CPU time required when using wall functions can be extremely important for the computation of complex three-dimensional flowfields.

One disadvantage of wall functions is that the log equation, which is fundamental to wall functions, is not accurate for some flowfields, such as those with regions of separated flow. Even with this limitation, wall functions have been shown to yield results comparable, and often superior, to those obtained with low-Reynolds-number models, including computations of some complex flowfields.[3,4,10–12]

Although it is straightforward to apply wall functions to simple geometries, difficulties arise when they are applied to complex geometries in generalized coordinate systems. In the Navier–Stokes equations, the shear stresses at the wall must be modified to reflect the values computed from the wall function equations. Although methods exist to do this for specific geometries and boundary conditions, they are not applicable to general geometries with wall heat transfer. A method is presented here that may be applied to generalized, curvilinear coordinates with nonorthogonal grids at walls, including cases with nonadiabatic walls. The present method is valid for points in the viscous sublayer as well as points in the log region.

Equations and Algorithm

The turbulence transport equations are nondimensionalized by the following reference quantities: velocity a_∞, density ρ_∞, viscosity μ_∞, length L, and time L/a_∞. In transformed coordinates, the equations are given by

$$\frac{\partial \hat{Q}_t}{\partial \tau} + \frac{\partial \hat{E}_t}{\partial \xi} + \frac{\partial \hat{F}_t}{\partial \eta} + \frac{\partial \hat{G}_t}{\partial \zeta} - Re^{-1}\left(\frac{\partial \hat{E}_{tv}}{\partial \xi} + \frac{\partial \hat{F}_{tv}}{\partial \eta} + \frac{\partial \hat{G}_{tv}}{\partial \zeta}\right) = \hat{H}_t \tag{1}$$

where the dependent variable vector is

$$\hat{Q}_t = J^{-1}\begin{bmatrix} \rho k \\ \rho \epsilon \end{bmatrix} \tag{2}$$

The flux vectors are

$$\hat{E}_t = J^{-1}\begin{bmatrix} U\rho k \\ U\rho \epsilon \end{bmatrix} \tag{3}$$

$$\hat{F}_t = J^{-1}\begin{bmatrix} V\rho k \\ V\rho \epsilon \end{bmatrix} \tag{4}$$

$$\hat{G}_t = J^{-1}\begin{bmatrix} W\rho k \\ W\rho \epsilon \end{bmatrix} \tag{5}$$

$$\hat{E}_{tv} = J^{-1}\begin{bmatrix} \mathcal{N}_k\left(\alpha_1\frac{\partial \rho k}{\partial \xi} + \alpha_4\frac{\partial \rho k}{\partial \eta} + \alpha_5\frac{\partial \rho k}{\partial \zeta}\right) \\ \mathcal{N}_\epsilon\left(\alpha_1\frac{\partial \rho \epsilon}{\partial \xi} + \alpha_4\frac{\partial \rho \epsilon}{\partial \eta} + \alpha_5\frac{\partial \rho \epsilon}{\partial \zeta}\right) \end{bmatrix} \tag{6}$$

$$\hat{F}_{tv} = J^{-1}\begin{bmatrix} \mathcal{N}_k\left(\alpha_4\frac{\partial \rho k}{\partial \xi} + \alpha_2\frac{\partial \rho k}{\partial \eta} + \alpha_6\frac{\partial \rho k}{\partial \zeta}\right) \\ \mathcal{N}_\epsilon\left(\alpha_4\frac{\partial \rho \epsilon}{\partial \xi} + \alpha_2\frac{\partial \rho \epsilon}{\partial \eta} + \alpha_6\frac{\partial \rho \epsilon}{\partial \zeta}\right) \end{bmatrix} \tag{7}$$

$$\hat{G}_{tv} = J^{-1}\begin{bmatrix} \mathcal{N}_k\left(\alpha_5\frac{\partial \rho k}{\partial \xi} + \alpha_6\frac{\partial \rho k}{\partial \eta} + \alpha_3\frac{\partial \rho k}{\partial \zeta}\right) \\ \mathcal{N}_\epsilon\left(\alpha_5\frac{\partial \rho \epsilon}{\partial \xi} + \alpha_6\frac{\partial \rho \epsilon}{\partial \eta} + \alpha_3\frac{\partial \rho \epsilon}{\partial \zeta}\right) \end{bmatrix} \tag{8}$$

where

$$\mathcal{N}_k = \frac{1}{\rho}\left(\mu + \frac{\mu_t}{\sigma_k}\right) \tag{9}$$

$$\mathcal{N}_\epsilon = \frac{1}{\rho}\left(\mu + \frac{\mu_t}{\sigma_\epsilon}\right) \tag{10}$$

$$\alpha_1 = \xi_x^2 + \xi_y^2 + \xi_z^2 \tag{11}$$

$$\alpha_2 = \eta_x^2 + \eta_y^2 + \eta_x^2 \tag{12}$$

$$\alpha_3 = \zeta_x^2 + \zeta_y^2 + \zeta_z^2 \tag{13}$$

$$\alpha_4 = \xi_x\eta_x + \xi_y\eta_y + \xi_z\eta_z \tag{14}$$

$$\alpha_5 = \xi_x\zeta_x + \xi_y\zeta_y + \xi_z\zeta_z \tag{15}$$

$$\alpha_6 = \eta_x\zeta_x + \eta_y\zeta_y + \eta_z\zeta_z \tag{16}$$

and the source term vector is

$$\hat{H}_t = J^{-1}\begin{bmatrix} \mathcal{P} - \rho\epsilon \\ C_1\frac{\epsilon}{k}\mathcal{P} - C_2\frac{\rho\epsilon^2}{k} \end{bmatrix} \tag{17}$$

where

$$\mathcal{P} = Re^{-1}\left[\mu_t\left(\frac{\partial u_i}{\partial x_j} + \frac{\partial u_j}{\partial x_i} - \frac{2}{3}\delta_{ij}\frac{\partial u_k}{\partial x_k}\right)\right]\frac{\partial u_i}{\partial u_j} - \frac{2}{3}\rho k\frac{\partial u_k}{\partial x_k} \tag{18}$$

The turbulent viscosity is given by

$$\nu_t = Re\left(c_\mu\frac{k^2}{\epsilon}\right) \tag{19}$$

For each time step, the Navier–Stokes equations are solved using a partially flux-split two-factor scheme.[13] The turbulence transport equations are then solved using a first-order upwind three-factor scheme. The source terms are fully linearized [including $\mu_t = \mu_t(k, \epsilon)$]. After each time step, any values of k and ϵ that are less than the freestream values are set to the freestream values to help prevent unphysical transient solutions. Additional details of the solvers are given by Sondak et al.[14]

Wall Functions

Wall function formulations consist of three basic steps. First, the friction velocity u_* and the wall shear stress τ_w are computed as functions of the mean flow variables. Values of k and ϵ are then computed at the grid point adjacent to the wall and are used for the boundary conditions for the turbulence transport equations. Finally, the wall shear stress from the first step is forced into the Navier–Stokes equations. It is this third step that proves nettlesome in generalized curvilinear coordinates.

A typical turbulent boundary-layer velocity profile is shown in Fig. 1. The incompressible form of the law of the wall will be used here for simplicity, although extension to the compressible form is straightforward.[15] In the log region, the velocity profile is given by

$$\frac{u}{u_*} = \frac{1}{\kappa}\ln\left(\frac{u_* y}{\nu}\right) + B \tag{20}$$

or in wall coordinates,

$$u^+ = \frac{1}{\kappa}\ln(y^+) + B \tag{21}$$

For the viscous sublayer,

$$\frac{u}{u_*} = \frac{u_* y}{\nu} \tag{22}$$

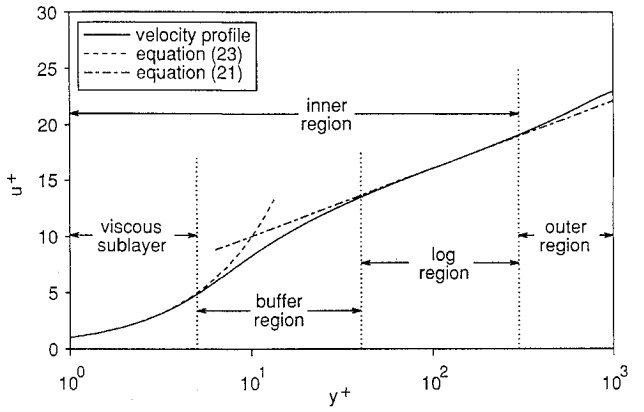

Fig. 1 Typical turbulent boundary-layer velocity profile.

or

$$u^+ = y^+ \tag{23}$$

The friction velocity and wall variables are defined by

$$u_* \equiv \sqrt{\frac{\tau_w}{\rho_w}} \tag{24}$$

$$u^+ \equiv \frac{u}{u_*} \tag{25}$$

and

$$y^+ \equiv \frac{u_* y}{\nu} \tag{26}$$

Using u and v from the previous time step, the friction velocity u_* can be calculated from Eq. (20) or Eq. (22), depending upon whether the grid point adjacent to the wall falls in the log region or the viscous sublayer. The appropriate equation is determined as follows. Referring to Fig. 1, Eqs. (23) and (21) may be seen to intersect at a single value of y^+, which will be called y_c^+. Neglecting the buffer region, y_c^+ delimits the viscous sublayer and the log region. From Eqs. (23) and (21),

$$y_c^+ = \frac{1}{\kappa} \ln(y_c^+) + B \tag{27}$$

This equation is solved for y_c^+ using Newton integration (to allow for various input values for κ and B). It is temporarily assumed that the point in question is in the viscous sublayer. Using the velocity and viscosity from the previous time step, Eq. (22) is solved for u_*, and y^+ is calculated from Eq. (26). If y^+ is less than y_c^+, the assumption that the point is in the viscous sublayer is correct. Otherwise, the point is actually in the log region, and u_* is recomputed from Eq. (20) using Newton iteration. The wall shear stress may then be computed by rearranging Eq. (24).

The next step is to set the boundary conditions for k and ϵ at the point adjacent to the wall. If the point is in the log region, it is assumed that the rate of production of turbulent kinetic energy is equal to the rate of dissipation, so

$$k = \frac{u_*^2}{\sqrt{c_u}} \tag{28}$$

and

$$\epsilon = \frac{(u_*^3}{\kappa y} \tag{29}$$

If the point is in the viscous sublayer, the assumption that production equals dissipation is not valid, and a different method must be employed. It can be shown that

$$k \propto y^2 \tag{30}$$

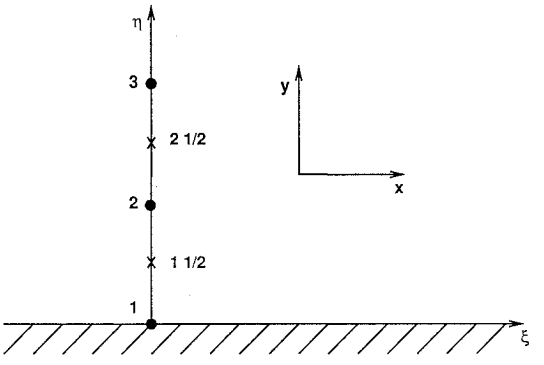

Fig. 2 Simple two-dimensional coordinate system.

near the wall.[16] The value of k is known at $y = y_c^+$ from Eq. (28) and is equal to zero at the wall due to the no-slip condition. Equation (30) therefore becomes

$$k = \frac{u_*^2}{\sqrt{c_\mu}} \left(\frac{y^+}{y_c^+} \right)^2 \tag{31}$$

This is similar to the method used by Gorski.[17] In deriving Eq. (31), it has been assumed that Eq. (30) is applicable throughout the viscous sublayer, even though this is strictly correct only very close to the wall. Additional computations will be required to determine whether or not this assumption causes significant errors, but the errors are expected to be small within the context of algebraic near-wall models.

An expression for ϵ is still needed for points in the viscous sublayer. Following Rodi,[8] the length scale equation of Norris and Reynolds[18] will be used,

$$l_\epsilon = \frac{c_l y}{1 + 5.3/Re_t} \tag{32}$$

where

$$c_l = \kappa c_\mu^{-3/4} \tag{33}$$

and

$$Re_t = \frac{\sqrt{ky}}{\nu} \tag{34}$$

Now that k and l_ϵ are known, ϵ may be computed from

$$\epsilon = \frac{k^{3/2}}{l_\epsilon} \tag{35}$$

Definition of the boundary conditions for k and ϵ is now complete.

The remaining step is to force the computed wall shear stress into the Navier–Stokes equations. A simple two-dimensional coordinate system for a boundary-layer flow with the ξ and η directions aligned with the x and y directions, respectively, is shown in Fig. 2. A sample diffusion term from the Navier–Stokes equations, $\partial \tau^{xy}/\partial \eta$, is approximated at point 2 by

$$\frac{\partial \tau^{xy}}{\partial \eta} \approx \tau^{xy}_{2\frac{1}{2}} - \tau^{xy}_{1\frac{1}{2}} \tag{36}$$

At point $1\frac{1}{2}$, the shear stress τ^{xy} is approximated by

$$\tau^{xy}_{1\frac{1}{2}} \approx (\mu + \mu_t)_{1\frac{1}{2}} \frac{u_2 - u_1}{y_2 - y_1} \tag{37}$$

Figure 3 shows a velocity profile on a grid with an exaggerated coarse spacing at the wall. The slope of the velocity profile at the wall will not be computed correctly, and Eq. (37) will not give a reasonable approximation to $\tau^{xy}_{2\frac{1}{2}}$.

One approach to solving this problem is to define an effective viscosity at the wall[19] such that the correct shear stress is obtained from Eq. (37), but this technique can result in errors in the energy

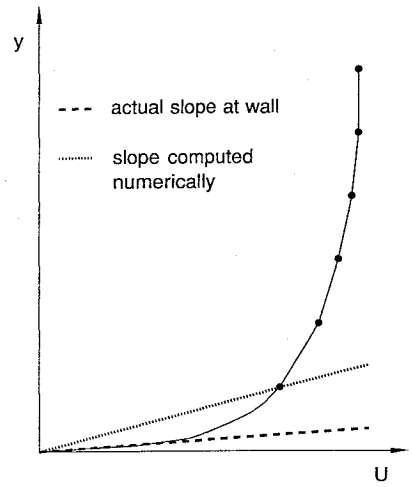

Fig. 3 Velocity profile with coarse wall spacing.

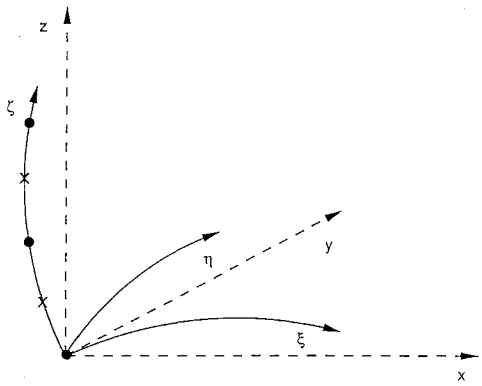

Fig. 4 General three-dimensional geometry.

equation. This may be seen by examining the heat transfer term in the energy equation,

$$q_i = -\left(\frac{\mu}{Pr} + \frac{\mu_t}{Pr_t}\right)\frac{\partial h}{\partial x_i} \tag{38}$$

where q_i is the i-direction heat transfer rate. The slope of the enthalpy profile will not be computed correctly numerically, for the same reason that was described earlier for the velocity profile. From the Reynolds analogy,

$$\frac{q_i}{\tau_{ij}} = \left[\left(\frac{\mu}{Pr} - \frac{\mu_t}{Pr_t}\right)\frac{\partial h}{\partial x_i}\right] \Big/ \left[(\mu + \mu_t)\frac{\partial u_j}{\partial x_i}\right] \tag{39}$$

If the ratio of the numerically computed slopes were equal to the actual ratio of the slopes, the same effective viscosity could be used in the momentum and energy equations. This is not, however, generally true.

To circumvent this problem, the shear stress deduced from the wall functions can be directly substituted for $\tau^{xy}_{1\frac{1}{2}}$ in Eq. (36), assuming a constant-stress layer near the wall. [The constant-stress assumption is consistent with the derivation of the law of the wall,[20] Eqs. (20) and (22).] An analogous substitution may be made for the heat transfer rate in the energy equation. This obviates the need to compute the slopes of the profiles.

This method becomes more complicated for general geometries, as shown in Fig. 4. The shear stress from the wall functions, τ_w, represents the shear stress acting parallel to the wall (in the ξ-η plane in Fig. 4) and is not equal to τ^{xy} as in the previous simple example. For the Navier–Stokes equations, the stress tensor in Cartesian coordinates (τ^{xx}, τ^{xy}, ...) is required. The following procedure will be used to compute this tensor. First, all components of the stress tensor will be computed in the conventional way using equations of the form of Eq. (37). This tensor is then transformed to a coordinate system with directions parallel and perpendicular to the wall, and physical components are computed in these directions. The shear stress τ_w is substituted for the appropriate physical components, and the transformation is reversed to obtain the required stress tensor. Details of these transformations will now be given.

Transformations

In generating grids for complex geometries, it is often difficult to maintain grid orthogonality at walls. In the following transformations, a coordinate direction perpendicular to the wall is required, so a new coordinate direction, called "γ," is defined in this direction. This new coordinate direction is used only in the shear stress transformations and not in the flow computation. An example coordinate system with the γ direction is shown in Fig. 5. In this example, the wall is defined by the ξ and η directions. Similar coordinate systems may be constructed for walls defined by the ξ-ζ and η-ζ directions, but, for simplicity, only the coordinate system in Fig. 5 will be dealt with here.

Metrics

First, metrics must be established in the new coordinate system. The covariant base vectors, which are the base vectors tangent to the coordinate directions, are given by

$$\mathbf{r}_\xi = (x_\xi, y_\xi, z_\xi) \tag{40}$$

$$\mathbf{r}_\eta = (x_\eta, y_\eta, z_\eta) \tag{41}$$

and

$$\mathbf{r}_\zeta = (x_\zeta, y_\zeta, z_\zeta) \tag{42}$$

The contravariant base vectors are

$$\nabla\xi = \frac{\mathbf{r}_\eta \times \mathbf{r}_\zeta}{\mathbf{r}_\xi \cdot \mathbf{r}_\eta \times \mathbf{r}_\zeta} \tag{43}$$

$$\nabla\eta = \frac{\mathbf{r}_\zeta \times \mathbf{r}_\xi}{\mathbf{r}_\xi \cdot \mathbf{r}_\eta \times \mathbf{r}_\zeta} \tag{44}$$

and

$$\nabla\zeta = \frac{\mathbf{r}_\xi \times \mathbf{r}_\eta}{\mathbf{r}_\xi \cdot \mathbf{r}_\eta \times \mathbf{r}_\zeta} \tag{45}$$

For a computational grid, the denominator of Eqs. (43–45) represents the volume of the grid cell or the reciprocal of the Jacobian of the coordinate transformation, J^{-1}.

From Eq. (45), it may be seen that $\nabla\zeta$ is perpendicular to the ξ and η directions. Since the covariant γ base vector,

$$\mathbf{r}_\gamma = (x_\gamma, y_\gamma, z_\gamma) \tag{46}$$

is also perpendicular to the ξ and η directions, $\nabla\zeta$ and $\mathbf{r}_\gamma$ are proportional to one another. Denoting the proportionality factor as b,

$$x_\gamma = b\zeta_x \tag{47}$$

$$y_\gamma = b\zeta_y \tag{48}$$

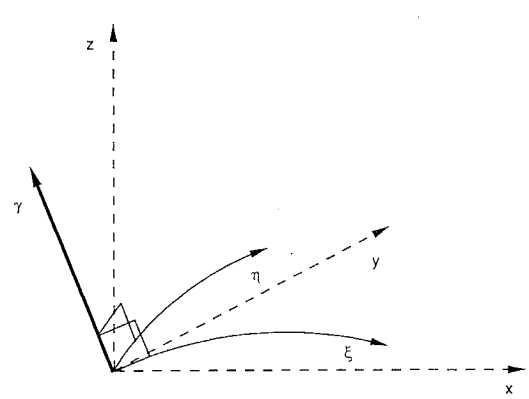

Fig. 5 γ coordinate direction.

and

$$z_\gamma = b\zeta_z \tag{49}$$

The γ direction has been defined, but magnitudes of the γ metrics still have to be established. In the example coordinate system of Fig. 5, an equation may be written analogous to Eq. (45),

$$\nabla\gamma = \frac{\mathbf{r}_\xi \times \mathbf{r}_\eta}{\mathbf{r}_\xi \cdot \mathbf{r}_\eta \times \mathbf{r}_\gamma} \tag{50}$$

Recall that the denominator of this equation is equal to J^{-1}. Since the values of the Jacobians will be available in (ξ, η, ζ) coordinates, the Jacobians in the (ξ, η, γ) coordinate system will be chosen to be equal to those in the old system. This is simply a convenience, so the computation of new Jacobians is not required. Comparing Eqs. (45) and (50), it may be seen that by setting the old and new Jacobians equal, the contravariant base vectors in the γ and ζ directions are also equal,

$$\gamma_x = \zeta_x \tag{51}$$

$$\gamma_y = \zeta_y \tag{52}$$

and

$$\gamma_z = \zeta_z \tag{53}$$

The term J^{-1} is given by

$$J^{-1} = \mathbf{r}_\xi \cdot \mathbf{r}_\eta \times \mathbf{r}_\gamma \tag{54}$$

Carrying out the vector operations,

$$J^{-1} = x_\xi(y_\eta z_\gamma - y_\gamma z_\eta) + y_\xi(x_\gamma z_\eta - x_\eta z_\gamma) + z_\xi(x_\eta y_\gamma - x_\gamma y_\eta) \tag{55}$$

Substituting Eqs. (47), (48), and (49) into Eq. (55) and solving for b give

$$b = \frac{J^{-1}}{x_\xi(y_\eta\zeta_z - \zeta_y\zeta_\eta) + y_\xi(\zeta_x z_\eta - x_\eta\zeta_z) + z_\xi(x_\eta\zeta_y - \zeta_x y_\eta)} \tag{56}$$

The metrics x_γ, y_γ, and z_γ may now be calculated from Eqs. (47–49). The remaining unknown contravariant base vectors are given by

$$\nabla\xi = \frac{\mathbf{r}_\eta \times \mathbf{r}_\gamma}{\mathbf{r}_\xi \cdot \mathbf{r}_\eta \times \mathbf{r}_\gamma} \tag{57}$$

and

$$\nabla\eta = \frac{\mathbf{r}_\gamma \times \mathbf{r}_\xi}{\mathbf{r}_\xi \cdot \mathbf{r}_\eta \times \mathbf{r}_\gamma} \tag{58}$$

The calculation of all of the metric quantities that are needed for the coordinate transformation is now complete.

Original Stress Tensor

The next step is to calculate the shear stresses in Cartesian (x, y, z) coordinates (e.g., τ^{xy}) at point $1\frac{1}{2}$ using the equation

$$\tau^{ij} = Re^{-1}(\mu + \mu_t)\left(\frac{\partial u_i}{\partial x_j} + \frac{\partial u_j}{\partial x_i} - \frac{2}{3}\delta_{ij}\frac{\partial u_k}{\partial x_k}\right) - \frac{2}{3}\delta_{ij}\rho k \tag{59}$$

These should be calculated in the same way that they are calculated in the discretized Navier–Stokes equations, i.e., the same averaging procedure should be used to obtain values at point $1\frac{1}{2}$, since some components may not be altered in the current procedure. The stresses are then transformed to the generalized coordinate system using the standard tensor transformation[21]

$$\breve{\tau}^{\alpha\beta} = \frac{\partial\gamma^\alpha}{\partial x^i}\frac{\partial\gamma^\beta}{\partial x^j}\tau^{ij} \tag{60}$$

Here, the $(\breve{})$ symbol represents quantities in the generalized coordinate system. For clarity, Greek letters are used for tensor indices in generalized coordinates, and Roman letters are used for tensor indices in Cartesian coordinates. The tensor x^i represents the Cartesian coordinate x, y, or z, and γ^α represents the generalized coordinate ξ, η, or γ.

Physical Components

The stresses $\breve{\tau}^{\alpha\beta}$ do not generally represent physical quantities, since the grid may be stretched in all directions. To obtain the physical components of the shear stresses in the generalized coordinate directions, we employ the following equation,[22]

$$\breve{\tau}(\alpha\beta) = \sqrt{\frac{\breve{\mathbf{g}}_{\alpha\alpha}}{\breve{\mathbf{g}}_{\beta\beta}}}\breve{\mathbf{g}}_{\beta\gamma}\breve{\tau}^{\alpha\gamma} \qquad \left(\text{no}\sum_{\alpha,\beta}\right) \tag{61}$$

where $\breve{\tau}(\alpha\beta)$ represents the physical components of the tensor. The metric tensor $\breve{\mathbf{g}}_{\alpha\beta}$ is given by

$$\breve{\mathbf{g}}_{\alpha\beta} = \frac{\partial x^i}{\partial\gamma^\alpha}\frac{\partial x^i}{\partial\gamma^\beta} \tag{62}$$

The physical velocity components in the generalized coordinate directions will also be needed:

$$\breve{u}(\alpha) = \breve{U}^\alpha\sqrt{\breve{\mathbf{g}}_{\alpha\alpha}} \qquad \left(\text{no}\sum_{\alpha}\right) \tag{63}$$

where $\breve{U}^\alpha$ represents the contravariant velocity components,

$$\breve{U}^\alpha = \frac{\partial\gamma^\alpha}{\partial x^i}u^i \tag{64}$$

Capital U is used for the contravariant velocity components, and lower case $\boldsymbol{u}$ is used for the physical velocity components in the Cartesian coordinate directions to be consistent with standard computational fluid dynamics (CFD) notation.

Inclusion of Wall Function Shear Stress

For three-dimensional geometries, the wall shear stress τ_w must be broken into components in the coordinate directions parallel to the wall (in the present example ξ and η). Scaling the shear stress components with the velocity components in the ξ and η directions gives

$$\breve{\breve{\tau}}(\xi\gamma) = \frac{\breve{u}(\xi)}{V_p}\tau_w \tag{65}$$

and

$$\breve{\breve{\tau}}(\eta\gamma) = \frac{\breve{u}(\eta)}{V_p}\tau_w \tag{66}$$

where V_p is the velocity component parallel to the wall, and τ_w is the wall shear stress from the wall functions. The symbol $(\breve{\breve{}})$ is used to indicate physical shear stress components that were deduced from the wall function equations, as opposed to those computed from Eq. (61). The physical shear stress components computed from Eq. (61) are now modified to reflect the wall function values. In the present example, $\breve{\tau}(\xi\gamma)$ and $\breve{\tau}(\eta\gamma)$ calculated in Eq. (61) are replaced by the values from Eqs. (65) and (66).

Reverse Transformation

Now that the shear stresses from the wall functions have been included, the previous procedure will be reversed to transform the new physical stresses in the generalized coordinate system to physical stresses in Cartesian coordinates. First, an equation is required to calculate tensor components from physical components, i.e., the inverse of Eq. (61). It is convenient here to work in matrix notation rather than with tensors. To express Eq. (61) in matrix notation, matrices will be defined as follows:

$$\boldsymbol{P} \equiv \begin{bmatrix} \tau(11) & \tau(12) & \tau(13) \\ \tau(21) & \tau(22) & \tau(23) \\ \tau(31) & \tau(32) & \tau(33) \end{bmatrix} \tag{67}$$

$$\boldsymbol{T} \equiv \begin{bmatrix} \tau^{11} & \tau^{12} & \tau^{13} \\ \tau^{21} & \tau^{22} & \tau^{23} \\ \tau^{31} & \tau^{32} & \tau^{33} \end{bmatrix} \tag{68}$$

Table 1 Summary of stress transformations

Step	Action	Variable	Eq.
1	Compute stresses in Cartesian coordinates	τ^{ij}	(59)
2	Transform stresses to generalized coordinates	$\breve{\tau}^{\alpha\beta}$	(60)
3	Compute physical components of stresses in generalized coordinate directions	$\breve{\tau}(\alpha\beta)$	(61)
4	Split wall shear stress into components parallel to the wall	$\breve{\breve{\tau}}(\xi\gamma)$, $\breve{\breve{\tau}}(\eta\gamma)$	(65), (66)
5	Substitute new shear stress components into physical stress matrix	$\breve{\breve{\boldsymbol{P}}}$	(74)
6	Compute stresses in generalized coordinates from physical components	$\breve{\breve{\boldsymbol{T}}}$	(73)
7	Compute new stresses in Cartesian coordinates	$\breve{\breve{\tau}}^{ij}$	(75)

$$\boldsymbol{G} \equiv \begin{bmatrix} g_{11} & g_{12} & g_{13} \\ g_{21} & g_{22} & g_{23} \\ g_{31} & g_{32} & g_{33} \end{bmatrix} \tag{69}$$

$$\boldsymbol{S} \equiv \begin{bmatrix} \sqrt{g_{11}} & 0 & 0 \\ 0 & \sqrt{g_{11}} & 0 \\ 0 & 0 & \sqrt{g_{33}} \end{bmatrix} \tag{70}$$

The ($\breve{}$) notation has been dropped, since these definitions hold for any coordinate system. Noting that the matrix $\boldsymbol{G}$ is symmetric, Eq. (61) may be written in matrix notation as

$$\boldsymbol{P} = \boldsymbol{S}\boldsymbol{T}(\boldsymbol{S}^{-1}\boldsymbol{G})^{T} \tag{71}$$

Solving for $\boldsymbol{T}$,

$$\boldsymbol{T} = \boldsymbol{S}^{-1}\boldsymbol{P}\left[(\boldsymbol{S}^{-1}\boldsymbol{G})^{T}\right]^{-1} \tag{72}$$

In the present example the new stress tensor may be computed from Eq. (72),

$$\breve{\breve{\boldsymbol{T}}} = \breve{\boldsymbol{S}}^{-1}\breve{\breve{\boldsymbol{P}}}\left[(\breve{\boldsymbol{S}}^{-1}\breve{\boldsymbol{G}})^{T}\right]^{-1} \tag{73}$$

where $\breve{\breve{\boldsymbol{P}}}$ is

$$\breve{\breve{\boldsymbol{P}}} = \begin{bmatrix} \breve{\tau}(\xi\xi) & \breve{\tau}(\xi\eta) & \breve{\breve{\tau}}(\xi\gamma) \\ \breve{\tau}(\eta\xi) & \breve{\tau}(\eta\eta) & \breve{\breve{\tau}}(\eta\gamma) \\ \breve{\breve{\tau}}(\gamma\xi) & \breve{\breve{\tau}}(\xi\eta) & \breve{\tau}(\gamma\gamma) \end{bmatrix} \tag{74}$$

Note that the stress components from Eqs. (65) and (66) have been substituted into the $\breve{\breve{\boldsymbol{P}}}$ matrix. Finally, returning to tensor notation ($\breve{\breve{\boldsymbol{T}}} = \breve{\breve{\tau}}^{\alpha\beta}$), the new stress tensor must be transformed to Cartesian coordinates,

$$\breve{\breve{\tau}}^{ij} = \frac{\partial x^{i}}{\partial \gamma^{\alpha}} \frac{\partial x^{j}}{\partial \gamma^{\beta}} \breve{\breve{\tau}}^{\alpha\beta} \tag{75}$$

In the Navier–Stokes equations, stresses adjacent to the wall, usually computed as in Eq. (37), are replaced by the new stress tensor $\breve{\breve{\tau}}^{ij}$. A summary of the procedure just described is shown in Table 1.

Results

Flat Plate

The first test case is the computation of incompressible, turbulent flow over a semi-infinite flat plate with zero pressure gradient. A skewed grid is used at the wall to test the procedure defining the γ coordinate direction. The grid is orthogonal to the plate at the inflow boundary. Moving downstream, the grid lines gradually become more and more skewed, until they reach an angle of 60 deg with respect to the plate. They remain at this angle for the rest of the domain. A close-up of the region of the grid near the wall is shown in Fig. 6.

This configuration was chosen for two reasons. First, if the grid were skewed at the inflow boundary, the boundary conditions would have been more difficult to implement. Also, some of the metrics (e.g., $\partial\zeta/\partial x$) are changing along the transformed coordinate directions, and so additional terms are brought into play in the computation.

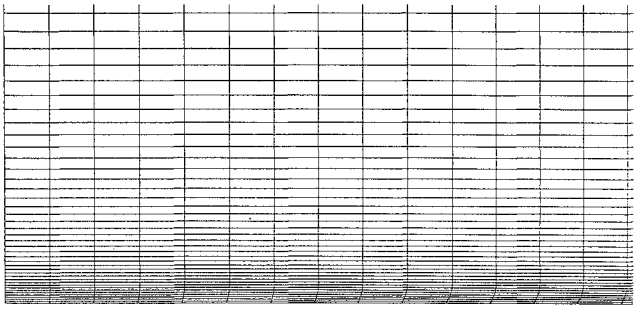

Fig. 6 Close-up of skewed flat plate grid near inflow boundary.

The freestream Mach number was set to 0.2 to minimize compressibility effects. The Reynolds number based on freestream velocity was 1×10^6 at the inflow boundary and 8×10^6 at the outflow boundary. The reference length was defined such that the distance from the virtual origin of the boundary layer to the inflow boundary was one unit of length. All lengths were normalized by this distance.

The wall spacing (distance from the wall to the grid line adjacent to the wall) was chosen such that $\Delta y_w^+ \approx 140$, which is well into the log region. The domain extended from 1 to 8 in the streamwise direction and from 0 to 1.5 in the normal direction. The location of the outer edge was chosen to exceed 10 times the estimated boundary-layer thickness at the downstream boundary. The grid was 101×61 (streamwise $\times$ normal).

An inflow streamwise velocity profile was specified using Coles' law of the wake[23] at $Re = 1 \times 10^6$. Note that the profile in the viscous sublayer was not required since wall functions were being used. At the inflow boundary, the normal velocity component was set to zero, the density was fixed at the freestream value, and the pressure was extrapolated (streamwise pressure gradient set to zero). At the outflow boundary, pressure was fixed at the freestream value, and density and both components of momentum were extrapolated. At the outer edge, density, both components of momentum, and pressure were extrapolated. At the wall, the velocity was set to zero, and density and pressure were extrapolated.

The inflow turbulence quantities were more difficult to estimate. Klebanoff[24] measured the turbulent kinetic energy profile for incompressible flow over a flat plate with zero streamwise pressure gradient at $Re = 4.2 \times 10^6$. These data were used to make a rough estimate of the distribution at the present $Re = 1 \times 10^6$. Correlations of C_f vs Re_x are readily available for this simple flow.[25] Using the estimated C_f, an estimate of u_* was obtained. The value of k at the grid point adjacent to the wall was computed from Eq. (28), and the entire Klebanoff distribution was scaled to match the computed value at this point. Finally, freestream values were cut off at $k/U_\infty^2 = 0.0002$, Klebanoff's approximate freestream k.

The inflow ϵ distribution was estimated using a method described by Launder et al.[26] The ratio of turbulent shear stress to turbulent kinetic energy was estimated to equal the constant 0.3. Since the k distribution was estimated earlier, the turbulent shear stress distribution

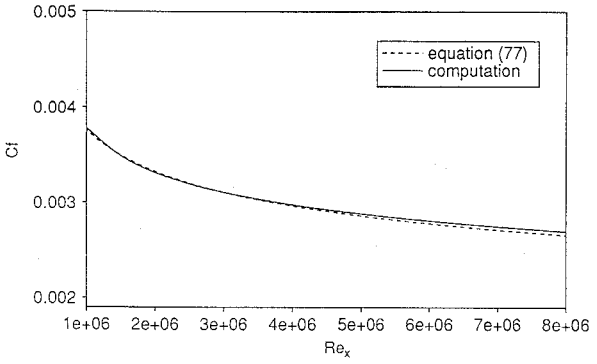

Fig. 7 Friction coefficient, flat plate, skewed grid.

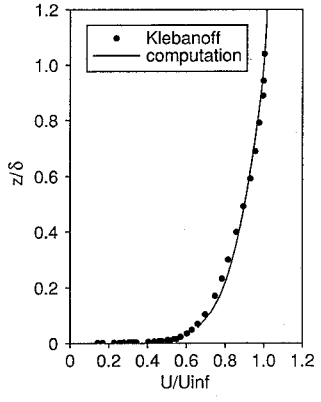

Fig. 8 Velocity profile, flat plate, skewed grid.

was also "known." The turbulent viscosity was then computed by rearranging the equation

$$\tau_t^{ij} = Re^{-1}(\mu_t)\left(\frac{\partial u_i}{\partial x_j} + \frac{\partial u_j}{\partial x_i} - \frac{2}{3}\delta_{ij}\frac{\partial u_k}{\partial x_k}\right) - \frac{2}{3}\delta_{ij}\rho k \qquad (76)$$

Equation (19) was then used to compute ϵ.

At the outflow boundary and the outer edge, k and ϵ were extrapolated. Values of k or ϵ are not required at the wall when using wall functions.

Since the friction coefficient is easily deduced from the friction velocity and the friction velocity is computed directly from the wall functions, comparison of friction coefficients is a good check on the effectiveness of a wall function formulation. An equation for the friction coefficient distribution for turbulent flow over a flat plate is given by[25]

$$Re_x = \frac{1}{12}\lambda^4 + \frac{e^{\kappa B}}{\kappa^3}\left[e^Z(Z^2-4Z+6) - 6 - 2Z - \frac{Z^4}{12} - \frac{Z^5}{20}\right] \qquad (77)$$

where

$$\lambda = \sqrt{2/C_f} \qquad (78)$$

and

$$Z = \kappa\lambda \qquad (79)$$

The computed results, shown in Fig. 7, are within 1.5% of the values from Eq. (77).

The computed velocity profile at $Re_x = 4.2 \times 10^6$ is compared with the Klebanoff test data in Fig. 8, where δ is the boundary-layer thickness and Unif is the freestream velocity. Again, the match is good.

Another test case was run identical to that previously discussed, but using an orthogonal grid throughout the domain. The results were indistinguishable from the skewed grid case.

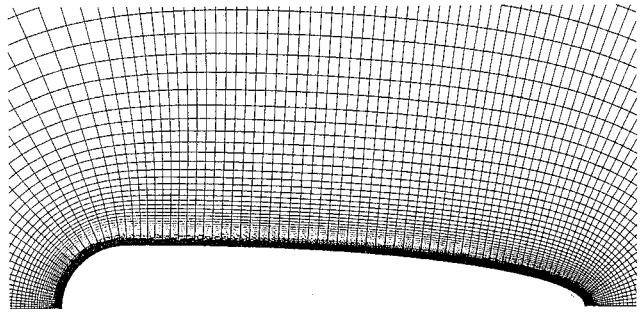

Fig. 9 Prolate hemispheroid, 101 × 104 grid.

Prolate Hemispheroid

The next step was to test the wall function formulation on a curved surface. A well-behaved (nonseparated) flowfield was desirable, since the purpose was to check the stress tensor transformations, and not yet to deal with the issue of the effectiveness of the present wall function formulation for separated flows.

Ramaprian et al.[27,28] measured surface pressures, friction coefficients, and velocity profiles for incompressible flow over a prolate hemispheroid with a hemispherical nose cap at zero and 10-deg angle of attack. The zero-degree angle of attack case was computed here using the k-ϵ model with the present wall function formulation as well as the Baldwin-Lomax[29] algebraic turbulence model and the Chien[2] low-Reynolds-number k-ϵ model.

The reference length for all distances in this section is the length of the body. The experimental Reynolds number based on freestream velocity was 2×10^6, and the freestream Mach number was approximately 0.06. The computations were run at the test Reynolds number, but the frestream Mach number was raised to 0.10 to avoid the incompressible limit of the code while still maintaining essentially incompressible flow. In the experiment, the boundary layer was tripped near the nose ($x = 0.04$), and the computations were therefore run completely turbulent.

Since the geometry was symmetrical, only half of the domain was solved. All grids were generated using the hyperbolic scheme of Chan and Steger.[30] Initially, an elliptic scheme was tried, but it proved impossible to maintain the desired wall spacing. The hyperbolic scheme permitted excellent control over wall spacing, ran extremely fast, and was easy to use.

A wall spacing was desired that would provide adequate resolution for the Baldwin-Lomax and Chien models without requiring an excessive number of grid points. A wall spacing of $\Delta y_w^+ \approx 4$ was chosen, resulting in a 101 × 104 (streamwise × normal) grid. This wall spacing would be somewhat coarse for many flows but proved sufficient for the present relatively simple flowfield. The wall-function cases were also run on a coarse grid, 101 × 80, with $\Delta y_w^+ \approx 48$. The grids were stretched geometrically normal to the body using a stretching ratio of 1.11. This relatively conservative value was chosen to minimize numerical errors due to grid stretching.

The body in the experiment was suspended by wires and therefore had no sting, so an o-grid was the natural choice for this configuration. The domain extends approximately 20 body lengths from the surface. A close-up of the grid is shown in Fig. 9. At the leading edge, $x = 0$, and at the trailing edge, $x = 1$. At the centerline of the body, $z = 0$.

At the outer edge of the domain, for inflow points, density and momentum components were fixed and pressure was extrapolated. At outflow points, pressure was fixed, and density and momentum components were extrapolated. At the axis, density and x momentum were extrapolated. The z momentum was set to zero due to symmetry. Flow along the axis streamline is irrotational, and so Bernoulli's equation was used to compute pressure. At the body surface, density and pressure were extrapolated, and momentum was set to zero.

At inflow points both k and ϵ were specified to freestream values, and at outflow points they were both extrapolated. At the axis, they were both also extrapolated. At the body surface the boundary conditions are part of the wall-function formulation. For the Chien model, k and ϵ were set to zero at the wall. Since the tunnel

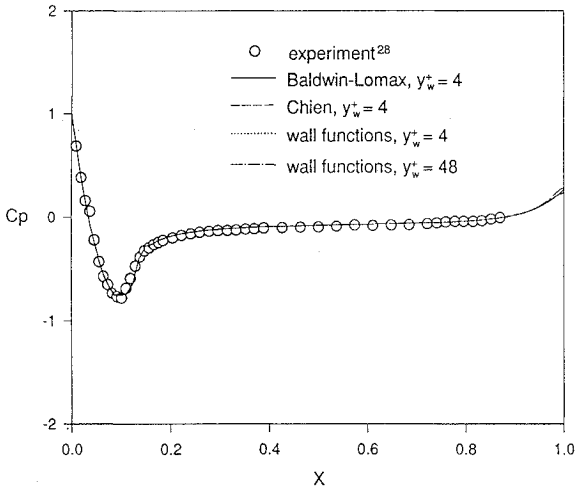

Fig. 10 Pressure coefficient, prolate hemispheroid.

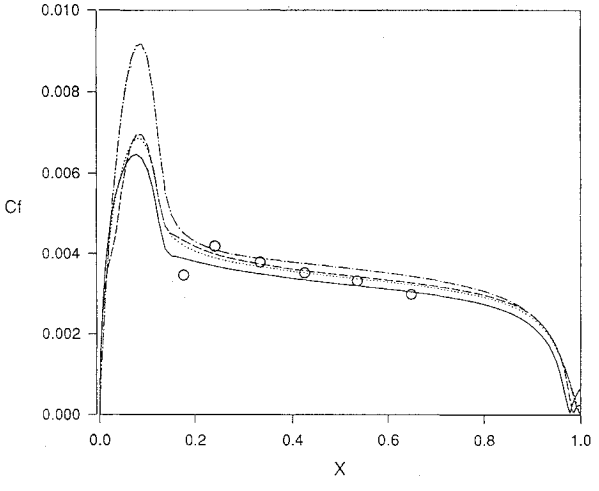

Fig. 11 Friction coefficient, prolate hemispheroid (see Fig. 10 for legend.)

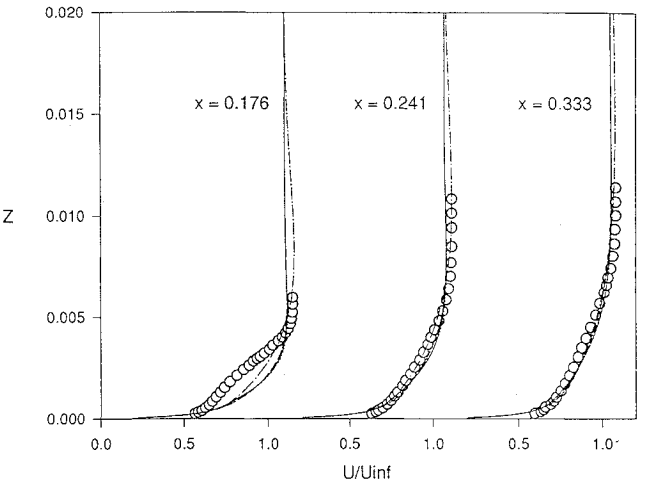

a)

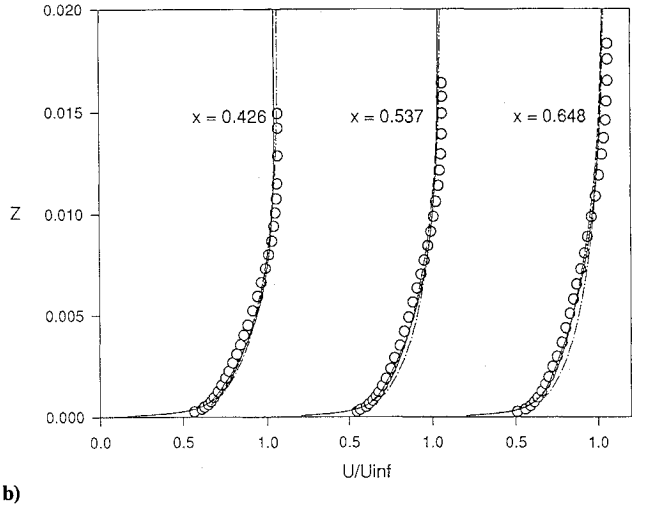

b)

Fig. 12 Velocity profiles, prolate hemispheroid (see Fig. 10 for legend.)

turbulence level was not measured in the experiment, a value of $k/U_\infty^2 = 0.005$ was assumed. A freestream turbulent viscosity of 0.1 (nondimensional) was assumed, and ϵ was calculated from Eq. (19). Experience has shown that there is latitude in selecting the value of the freestream turbulence level and turbulent viscosity without affecting the solution.

Computed boundary-layer profiles are often affected adversely by even modest amounts of smoothing.[31] Since the physical shear stresses become large near walls, smoothing may be decreased in this region without causing the computation to become unstable. Various techniques of gradually reducing the smoothing near the wall were tried, but the best solution was to simply set the smoothing equal to zero at the seven grid points adjacent to the wall. The number of grid points at which the smoothing may be set to zero is a function of the flowfield, and it should not be construed that the number seven is optimal in any sense.

The computed pressure coefficient distribution is compared with the experimental data in Fig. 10. All turbulence models give good results, including the wall-function solution on the coarse grid.

Friction coefficients [$c_f = 2\tau_w/(\rho_\infty u_\infty^2)$] are shown in Fig. 11. For the wall-function cases, the friction coefficients were calculated from the known shear stress. For the other two models, $\tau_w \approx \mu \partial V/\partial n$, where V is the velocity magnitude and n is the normal distance from the wall. The results from all three models compare well with the test data with the exception of the first measurement station. The first measurement station is located in a region of adverse pressure gradient immediately after the flow accelerates over the nose in a strongly favorable pressure gradient, and this is a difficult situation for any turbulence model to simulate accurately. As will be seen in subsequent plots, none of the models reproduce the character of the velocity distribution very well at the first measurement station. It is also possible that the flow relaminarized after being tripped near the stagnation point in the experiment. This would explain the fact that the measured friction coefficient is lower than the computed values at the first measurement station. The velocity distributions are shown in Fig. 12. Results from all models compare reasonably well with the test data. More importantly, the wall function solution is very close to the solution from the other two models. It should be kept in mind that the grid point adjacent to the wall lies in or near the viscous sublayer and not in the log region. In this respect, it may be thought of as a "worst case" test for the present wall functions. The coarse-grid solution shows some deviation from the fine-grid solutions, but the differences are not large. In the 101 × 80 grid, the point adjacent to the wall is in the log region, whereas this is not true for the finger grid, and so the boundary conditions for k and ϵ are computed differently for the two cases [Eqs. (28) and (29) vs Eqs. (31) and (35)]. Also, even when using wall functions, there is a limit to the coarseness of the grid that may be employed while still resolving features of the boundary layer. The coarse grid case may be pushing that limit.

Conclusions

A method has been developed for the application of wall functions to generalized curvilinear coordinates with nonorthogonal grids. It has been tested on a flat surface with a nonorthogonal grid and a curved surface with an orthogonal grid.

For flow over the prolate hemispheroid, the k-ϵ model with the wall function formulation, the Baldwin-Lomax algebraic model, and the Chien low-Reynolds-number k-ϵ model all gave good results for the fine-grid case. For the case with larger grid spacing at the wall, the wall-function solution still gave good results, demonstrating the

effectiveness of the technique used to handle points in both the log region and the viscous sublayer.

It is well known that the k-ϵ model requires attention for flows with strong adverse pressure gradients and streamline curvature. Various modifications have been proposed.[32–35] The application of such enhancements has the potential to improve the solution at the first measurement station. The use of wall functions on curved surfaces should not pose any problems, since the law of the wall has been observed to hold close to both convex and concave surfaces.[36]

Acknowledgment

The authors gratefully acknowledge the support provided for this study by NASA Ames Research Center under Interchange NCA2-526.

References

[1]Jones, W. P., and Launder, B. E., "The Prediction of Laminarization with a Two-Equation Model of Turbulence," *International Journal of Heat Transfer*, Vol. 15, Feb. 1972, pp. 301–314.

[2]Chien, K.-Y., "Predictions of Channel and Boundary-Layer Flows with a Low-Reynolds-Number Turbulence Model," *AIAA Journal*, Vol. 20, No. 1, 1982, pp. 33–38.

[3]Viegas, J. R., and Rubesin, M. W., "Wall-Function Boundary Conditions in the Solution of the Navier–Stokes Equations for Complex Compressible Flows," AIAA Paper 83-1694, July 1983.

[4]Chieng, C. C., and Launder, B. E., "On the Calculation of Turbulent Heat Transport Downstream from an Abrupt Pipe Expansion," *Numerical Heat Transfer*, Vol. 3, 1980, pp. 189–207.

[5]Patel, V. P., Rodi, W., and Scheuerer, G., "Turbulence Models for Near-Wall and Low Reynolds Number Flows: A Review," *AIAA Journal*, Vol. 23, No. 9, 1985, pp. 1308–1319.

[6]Bernard, P. S., "Limitations of the Near-Wall k-eps Turbulence Model," *AIAA Journal*, Vol. 24, No. 4, 1986, pp. 619–622.

[7]Lewis, J. P., and Pletcher, R. H., "A Boundary-Layer Computational Model for Predicting the Flow and Heat Transfer in Sudden Expansions," Iowa State Univ. College of Engineering, TR HTL-41, CFD-14, Ames, IA, July 1986.

[8]Rodi, W., "Experience with Two-Layer Models Combining the k-ϵ Model with a One-Equation Model Near the Wall," AIAA Paper 91-0216, Jan. 1991.

[9]Horstman, C. C., "Hypersonic Shock-Wave Turbulent Boundary-Layer Interactions Flows—Experiment and Computation," AIAA Paper 91-1760, June 1991.

[10]Viegas, J. R., Rubesin, M. W., and Horstman, C. C., "On the Use of Wall Functions as Boundary Conditions for Two-Dimensional Separated Compressible Flows," AIAA Paper 85-0180, Jan. 1985.

[11]Chen, H. C., and Patel, V. C., "Practical Near-Wall Turbulence Models for Complex Flows Including Separation," AIAA Paper 87-1300, June 1987.

[12]Avva, R., Smith, C., and Singhal, A., "Comparative Study of High and Low Reynolds Number Versions of k-e Models," AIAA Paper 90-0246, Jan. 1990.

[13]Ying, S. X., Steger, J. L., Schiff, L. B., and Baganoff, D., "Numerical Simulation of Unsteady, Viscous, High-Angle-of-Attack Flows Using a Partially Flux-Split Algorithm," AIAA Paper 86-2179, Aug. 1986.

[14]Sondak, D. L., Pletcher, R. H., and Van Dalsem, W. R., " Wall Functions for the k-ϵ Turbulence Model in Generalized Curvilinear Coordinates," Iowa State Univ. College of Engineering, TR HTL-41, CFD-14, Ames, IA, May 1992.

[15]Bradshaw, P., "Compressible Turbulent Shear Layers," *Annual Review of Fluid Mechanics*, Vol. 9, 1977, pp. 33–54.

[16]Launder, B. E., "Second-Moment Closure: Methodology and Practice," *Turbulence Models and Their Applications*, Vol. 2, Editions Eyrolles, Paris, 1984.

[17]Gorski, J. J., "A New Near-Wall Formulation for the k-ϵ Equations of Turbulence," AIAA Paper 86-0556, Jan. 1986.

[18]Norris, H. L., and Reynolds, W. C., "Turbulent Channel Flow with a Moving Wavy Boundary," Stanford Univ. Dept. of Mechanical Engineering, TR TF-7, Stanford, CA, 1975.

[19]Huang, P. G., and Coakley, T. J., "Calculations of Supersonic and Hypersonic Flows Using Compressible Wall Functions," 2nd International Symposium on Turbulence Modelling and Measurements, Florence, Italy, May 31–June 2, 1993.

[20]Cebeci, T., and Smith, A. M. O., *Analysis of Turbulent Boundary Layers*, Academic Press, New York, 1974.

[21]Sokolnikoff, I. S., *Tensor Analysis Theory and Applications to Geometry and Mechanics of Continua*, 2nd ed., Wiley, New York, 1964.

[22]Aris, R., *Vectors, Tensors, and the Basic Equations of Fluid Mechanics*, Prentice-Hall, Englewood Cliffs, NJ, 1962.

[23]Coles, D. E., "The Law of the Wake in the Turbulent Boundary Layer," *Journal of Fluid Mechanics*, Vol. 1, 1956, pp. 191–226.

[24]Klebanoff, P. S., "Characteristics of Turbulence in a Boundary Layer with Zero Pressure Gradient," NACA Rept. 1247, 1955.

[25]White, F. M., *Viscous Fluid Flow*, McGraw-Hill, New York, 1974.

[26]Launder, B. E., Morse, A., Rodi, W., and Spalding, D. B., "Prediction of Free Shear Flows—A Comparison of the Performance of Six Turbulence Models," *Free Turbulent Shear Flows: Proceedings of a Conference Held at NASA Langley Research Center* (Hampton, VA), NASA SP-321, 1972.

[27]Ramaprian, B. R., Patel, V. C., and Choi, D. H., "Mean Flow Measurements in the Three-Dimensional Boundary Layer over a Body of Revolution at Incidence," Iowa Inst. of Hydraulic Research, Univ. of Iowa, IIHR Limited Distribution Rept. 56, Iowa City, IA, 1978.

[28]Ramaprian, B. R., Patel, V. C., and Choi, D. H., "Mean Flow Measurements in the Three-Dimensional Boundary Layer over a Body of Revolution at Incidence," *Journal of Fluid Mechanics*, Vol. 103, 1981, pp. 479–504.

[29]Baldwin, B. S., and Lomax, H., "Thin Layer Approximation and Algebraic Model for Separated Turbulent Flows," AIAA Paper 78-257, Jan. 1978.

[30]Chan, W., and Steger, J., "A Generalized Scheme for Three-Dimensional Hyperbolic Grid Generation," AIAA Paper 91-1588, June 1991.

[31]Kaynak, Ü., and Flores, J., "Advances in the Computation of Transonic Separated Flows over Finite Wings," AIAA Paper 87-1195, June 1987.

[32]Launder, B. E., Priddin, C. H., and Sharma, B. I., "The Calculation of Turbulent Boundary Layers on Spinning and Curved Surfaces," *ASME Journal of Fluids Engineering*, Vol. 99, 1977, pp. 231–239.

[33]Hanjalic, K., and Launder, B. E., "Sensitizing the Dissipation Equation to Irrotational Strains," *ASME Journal of Fluids Engineering*, Vol. 102, 1980, pp. 34–40.

[34]Rodi, W., and Scheuerer, G., "Calculation of Curved Shear Layers with Two-Equation Turbulence Models," *Physics of Fluids*, Vol. 26, No. 6, 1983, pp. 1422–1436.

[35]Pourahmadi, F., and Humphrey, A. C., "Prediction of Curved Channel Flow with an Extended k-ϵ Model of Turbulence," *AIAA Journal*, Vol. 21, No. 10, 1983, pp. 1365–1373.

[36]Moser, R. D., and Moin, P., "The Effects of Curvature in Wall-Bounded Turbulent Flows," *Journal of Fluid Mechanics*, Vol. 175, 1987, pp. 479–510.